*Inorganica Chimica Acta*, *144* (1988) 275–280



# Stability Trends and Fragmentation Patterns of Gaseous Yttrium Oxide Clusters Studied by Fast Atom Bombardment Tandem Mass Spectrometry

ISHENKUMBA A. KAHWA* and JOEL SELBIN**

*Chemistry Department, Louisiana State University, Baton Rouge, La. 70803, U.S.A.*

THOMAS C.-Y. HSIEH

*Food Science Department, Louisiana State University and LSU Agricultural Center, Baton Rouge, La. 70803, U.S.A.*

DAVID W. EVANS, KRISHNA M. PAMIDIMUKKALA and ROGER LAINE

*Biochemistry Department, Louisiana State University, Baton Rouge, La. 70803, U.S.A.*

(Received September 4, 1987)

## Abstract

The fragmentation patterns of yttrium oxide cluster species $YO^+$, $Y_2O_2^+$, $Y_2O_3^+$, $Y_3O_4^+$, $Y_4O_6^+$, $Y_5O_7^+$, $Y_6O_8^+$ and $Y_7O_{10}^+$ were investigated at collision energies 30–110 and 170 eV by fast atom bombardment tandem mass spectrometry. The collision activated dissociation (CAD) spectra obtained revealed higher thermodynamic stability for the clusters of general formula $Y_aO_{(3a-1)/2}^+$, where $a$ is an odd number (e.g. $YO^+$, $Y_3O_4^+$, $Y_5O_7^+$, $Y_7O_{10}^+$) which are also the preferred CAD products for all oxide clusters studied. These most stable oxides are constituted by trivalent yttrium only whereas those containing formally tetravalent yttrium $Y_aO_{3a/2}^+$, (where $a$ is even) e.g. $Y_2O_3^+$ and $Y_4O_6^+$, are extremely unstable. The clusters $Y_aO_{(3a-2)/2}^+$, (where $a$ is even) containing divalent yttrium, e.g. $Y_2O_2^+$ and $Y_6O_8^+$, have considerable stability but their CAD products are again the thermodynamic products $Y_aO_{(3a-1)/2}^+$. Electronic structures appear to have overriding significance in determining the thermodynamic stabilities of the oxide cluster species.

## Introduction

We have recently reported the detection of gaseous polyoxo polylanthanide clusters in a fast atom bombardment mass spectrometer (FAB MS) [1–3]. Those lanthanide (Ln) oxo clusters constitute four major homologous series, namely, $Ln_aO_{(3a-1)/2}^+$ where $a$ is odd, e.g. $Ln_9O_{13}^+$, $Ln_7O_{10}^+$, $Ln_5O_7^+$, $Ln_3O_4^+$ and $LnO^+$; $Ln_aO_{3a/2}^+$ where $a$ is even, e.g. $Ln_8O_{12}^+$, $Ln_6O_9^+$, $Ln_4O_6^+$ and $Ln_2O_3^+$; $Ln_aO_a^+$, where $a$ is any integer larger than 1, e.g. $Ln_2O_2^+$, $Ln_3O_3^+$ and $Ln_4O_4^+$; and $Ln_aO_{(3a-2)/2}^+$ where $a$ is even, e.g. $Ln_2O_2^+$, $Ln_4O_5^+$, $Ln_6O_8^+$ and $Ln_8O_{11}^+$ [1–3]. The homologous series $Ln_aO_{(3a-1)/2}^+$, the members of which are the most prominent in the FAB MS spectra of lanthanide compounds [1, 3], are derived from successive additions of $Ln_2O_3$ to $LnO^+$. The series $Ln_aO_{3a/2}^+$ and $Ln_aO_{(3a-2)/2}^+$ are derived from successive additions of $Ln_2O_3$ to $Ln_2O_3^+$ and $Ln_2O_2^+$ respectively. The series of reduced oxides $Ln_aO_a^+$ is apparently derived by adding successively LnO to $LnO^+$ and is typical of the FAB MS spectra of europium and ytterbium compounds in which the rare earth atom has a readily accessible divalent state [1, 3].

Although group IIIA elements, aluminium, gallium and indium did not yield gaseous oxide clusters similar to those of lanthanides in a relatively cool FAB MS sample holder [1, 3], a recent study of vitreous boron oxide $B_2O_3$(s) in a specially designed high temperature FAB MS sample holder [4, 5] has yielded oxides similar to those of lanthanides. As with the oxide clusters $Ln_aO_{(3a-1)/2}^+$, the boron oxide species $B_aO_{(3a-1)/2}^+$ were the most prominent in that high temperature FAB MS study. Therefore, despite vast differences in the bonding behavior of boron and the rare earths in the solid and liquid states, their gas phase metal–oxygen chemistry appears to be similar.

The ratio of oxygen to lanthanide atoms in all the oxides is rather small and leaves high coordinative unsaturation on lanthanide cations which generally prefer large coordination numbers defined by undirected bonds [6, 7]. It was therefore interesting to determine the influence of the coordinative unsaturation and unusual oxidation states associated with gaseous oxide species on their thermodynamic stabilities and fragmentation patterns.

We herein report the stability trends and fragmentation patterns of various gaseous yttrium oxide

*On study leave from Chemistry Department, University of Dar es Salaam, P.O. Box 35061, Dar es Salaam, Tanzania.

**Author to whom correspondence should be addressed.

0020-1693/88/$3.50

cluster cations and a qualitative electronic rationale for the greater thermodynamic stability of $Y_aO_{(3a-1)/2}^+$ species.

## Experimental

Samples used in these studies were the same as those reported previously [1].

A TSQ70 Finnigan Mat triple stage quadrupole mass spectrometer equipped with FAB MS/MS capability was used to obtain the collision activated dissociation spectra (CAD) of the ions $YO^+$, $Y_2O_2^+$, $Y_2O_3^+$, $Y_3O_4^+$, $Y_4O_6^+$, $Y_5O_7^+$, $Y_6O_8^+$ and $Y_7O_{10}^+$. The ions were selected in the first quadrupole, collided with flowing argon in the second quadrupole (first field free region) and the fragmentation ion beam was analyzed in the third quadrupole. It was not necessary to use glycerol in order to generate the oxide cations. Cesium iodide and glycerol were used to calibrate both the first and the third quadrupole systems.

The daughter ion spectra were acquired with collision offset potentials set at −30, −50, −70, −90, −110 and −170 V.

## Results

The collision activated dissociation processes of the cations $Y_7O_{10}^+$, $Y_5O_7^+$, $Y_3O_4^+$, $Y_2O_3^+$, $Y_2O_2^+$ and $YO^+$ are summarized in Figs. 1–7, in which the intensities of the daughter ions are plotted against collision energies of the parent ion. Each of the data points used to make the plots was obtained from an average spectrum of at least 20 scans.

### *CAD of $Y_7O_{10}^+$*

Figure 1 shows the collision activated dissociation (CAD) products of $Y_7O_{10}^+$ at various collision energies and their intensities relative to the intensity of the base peak, namely $Y_7O_{10}^+$. There are no well defined relationships between the intensities of the daughter ions $Y_5O_7^+$ and $Y_3O_4^+$ with collision energy of $Y_7O_{10}^+$. But the intensities of $Y_3O_4^+$, which is the major CAD product and $Y_5O_7^+$ the minor product, clearly increase with collision energy. The parent ion $Y_7O_{10}^+$ and the daughter ions $Y_5O_7^+$ and $Y_3O_4^+$ belong to the oxide cluster class $Y_aO_{(3a-1)/2}^+$. The daughter ions are thus formed by loss of $(Y_2O_3)_n$ as:

$$Y_7O_{10}^+ \xrightarrow{-Y_2O_3} Y_5O_7^+ \quad (1)$$

$$Y_7O_{10}^+ \xrightarrow{-Y_4O_6} Y_3O_4^+ \quad (2)$$

Although the daughter ions $Y_5O_7^+$ and $Y_3O_4^+$ have the same appearance potential (*i.e.* reactions 1 and 2 have the same activation energy), formation of $Y_3O_4^+$ is the preferred CAD route for $Y_7O_{10}$. The ions $Y_2O_3^+$ and $Y_4O_6^+$ do not show up in the daughter ion spectra except at high collision energies. It is therefore reasonable to assume that they are formed as neutrals and may be ionized in subsequent collisions if they separate from $Y_7O_{10}^+$ with sufficient kinetic energy. At collision energy 170 eV the species $Y_2O_2^+$ (6%), $Y_2O_3^+$ (7%), $Y_4O_6^+$ (11%) and $Y_6O_8^+$ (7%) are observed in addition to $Y_3O_4^+$ (85%), $Y_5O_7^+$ (7%) and $Y_7O_{10}^+$ (100%). CAD reaction (2) increases dramatically at collision energies higher than 90 eV (Fig. 1).

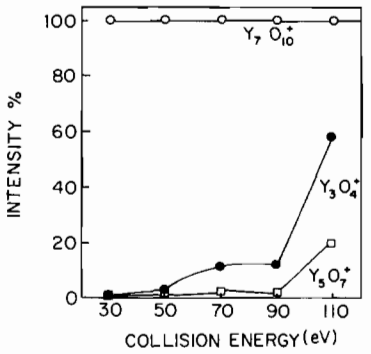


Fig. 1. Average CAD spectra of $Y_7O_{10}^+$: intensities of parent and daughter ions *vs.* collision energy of $Y_7O_{10}^+$.

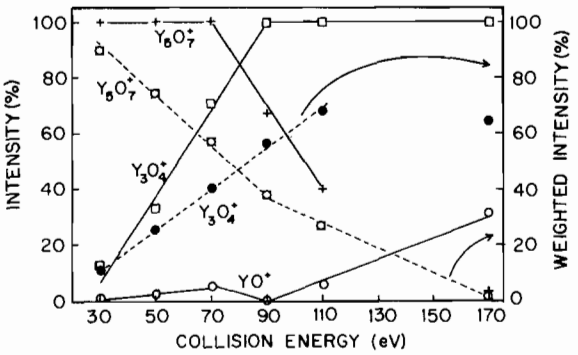


Fig. 2. Average CAD spectra of $Y_5O_7^+$: intensities (solid lines) and weighted intensity (broken lines) of daughter and parent ions *vs.* collision energy of $Y_5O_7^+$.

### *CAD of $Y_5O_7^+$*

The collision activated dissociation products of the ion $Y_5O_7^+$ are mainly $YO^+$ and $Y_3O_4^+$ (Fig. 2). Minor products at a collision energy of 170 eV and their intensities were $Y_2O_2^+$ (17%), $Y_2O_3^+$ (4%) and $Y_4O_5^+$ (9%). The intensity of the major CAD product $Y_3O_4^+$ increases linearly to 100% in the collision energy range 30–90 eV, which is consistent with a single unimolecular CAD process leading to $Y_3O_4^+$. The intensity of $YO^+$ also increases linearly with collision energy suggesting that $YO^+$ is as well predominantly produced from a single process. The

parent ion $Y_5O_7^+$ and its daughter ions $YO^+$ and $Y_3O_4^+$ belong to the oxide cluster class $Y_aO_{(3a-1)/2}^+$. The daughter ions may be derived from the parent ion by elimination of $(Y_2O_3)_n$ $n = 1, 2$ as:

$$Y_5O_7^+ \xrightarrow{-Y_2O_3} Y_3O_4^+ \quad (3)$$

$$Y_5O_7^+ \xrightarrow{-Y_4O_6} YO^+ \quad (4)$$

Unlike the CAD of $Y_7O_{10}^+$ in which loss of $Y_4O_6$ is preferred, CAD of $Y_5O_{10}^+$ exhibits preference for elimination of $Y_2O_3$ to form $Y_3O_4^+$ (reactions 2 and 3). The appearance potentials of $YO^+$ and $Y_3O_4^+$ from $Y_5O_7^+$ are about the same; therefore intensity differences arise from differentials in the kinetics of reactions (3) and (4). The $(Y_2O_3)_n$ products or their derivatives do not show up in the daughter ion spectra except at high parent ion collision energies (170 eV) as found in CAD of $Y_7O_{10}^+$. Multiple decay processes for $Y_5O_7^+$ are indicated by a non-linear relationship of the intensity of $Y_5O_7^+$ and collision energy at high energies (Fig. 2). When the intensities of all the CAD products and that of the parent ion ($Y_5O_7^+$) are summed up and the intensity of the parent ion is expressed as a percentage of this total, two linear relationships between such weighted intensities and collision energy are observed (Fig. 2). There is a fast linear $Y_5O_7^+$ decay with increasing collision energy at 30–90 eV. Thereafter, a slower linear decay sets in which suggests a change in the CAD mechanism. These observations are consistent with an initially dominant reaction (3) and an increasingly significant reaction (4) at high energies (Fig. 2).

*CAD of $Y_3O_4^+$*

The daughter ions of $Y_3O_4^+$ (Fig. 3) are mainly $YO^+$ and the less abundant $Y_2O_2^+$ and $Y_2O_3^+$ the occurrence and intensity of which are collision energy dependent. The intensity of $YO^+$ rises rapidly and linearly to 100% in the collision energy range 30–70 eV. The intensity of $Y_2O_3^+$ rises linearly but much more slowly. The intensity of $Y_2O_2^+$ is curvilinear indicating more complex formation processes (eqns. (7) and (8)).

The major CAD product $YO^+$ may be derived from $Y_3O_4^+$ via elimination of neutral $Y_2O_3$:

$$Y_3O_4^+ \xrightarrow{-Y_2O_3} YO^+ \quad (5)$$

If the neutral species $Y_2O_3$ leaves the parent ion $Y_3O_4^+$ with sufficient kinetic energy and subsequently collides with argon, ionization may occur:

$$Y_2O_3 \longrightarrow Y_2O_3^+ + e^- \quad (6)$$

or the molecule may undergo dissociative ionization as:

$$Y_2O_3 \longrightarrow Y_2O_2^+ + O^- \quad (7)$$

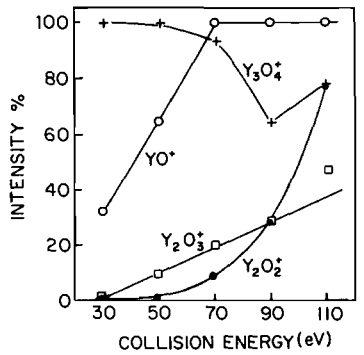


Fig. 3. Average CAD spectra of $Y_3O_4^+$: intensities of parent and daughter ions *vs.* collision energy of $Y_3O_4^+$.

The species $Y_2O_2^+$ may also be obtained directly from $Y_3O_4^+$ by the dissociation process:

$$Y_3O_4^+ \longrightarrow Y_2O_2^+ + YO^+ + O^- \quad (8)$$

Reaction (5), however, has the lowest activation energy on the basis of a low appearance potential of $YO^+$ (≃15 eV) (*vide infra*). The processes yielding $Y_2O_2^+$ are more favored by increasing collision energy of the parent ion $Y_3O_4^+$ (Fig. 3). This is seen more clearly when the intensity ratio $\theta$ (intensity of $Y_2O_2^+$/intensity of $Y_2O_3^+$) is plotted against the collision energy (Fig. 4 inset). But this does not identify either one of reactions (7) and (8) as being the dominant one. However, the fact that reaction (5) is dominant at low collision energies (30–90 eV) whereas reaction (8) is dominant at high collision energies (90–170 eV) is evident when intensities of the oxide ions $Y_3O_4^+$, $Y_2O_3^+$, $Y_2O_2^+$ and $YO^+$ are summed up and each is expressed as a percentage of this sum (Fig. 4). A plot of such weighted intensities against collision energies (Fig. 4) reveals that $Y_3O_4^+$ undergoes two different CAD mechanisms: a fast one in the range 30–90 eV, and a slower one in the range 90–170 eV. The onset of the slower one coincides with a drop in the weighted intensity of $Y_2O_3^+$ and probably a leveling off of the weighted intensity of $Y_2O_2^+$. The collision energy dependencies

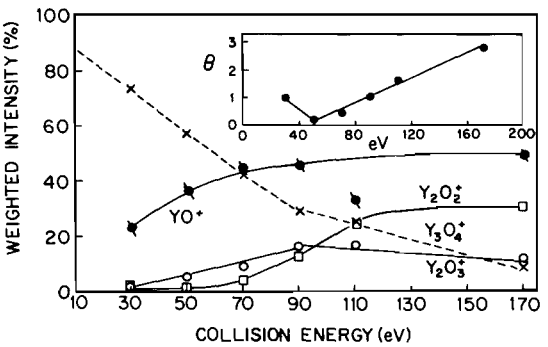


Fig. 4. Average CAD spectra of $Y_3O_4^+$: weighted intensities of daughter and parent ions *vs.* collision energy of $Y_3O_4^+$.

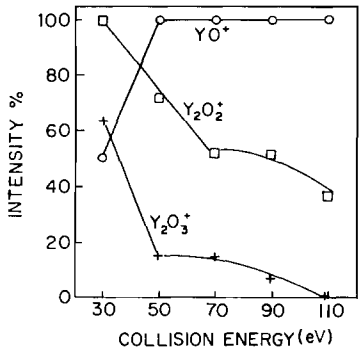


Fig. 5. Average CAD spectra of $Y_2O_3^+$: intensities of daughter and parent ions *vs.* collision energy of $Y_2O_3^+$.

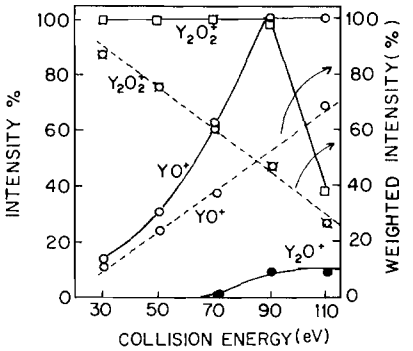


Fig. 6. Average CAD spectra of $Y_2O_2^+$: intensities (solid lines) and weighted (broken lines) intensities of daughter and parent ions *vs.* collision energy of $Y_2O_3^+$.

of weighted intensities of $YO^+$ and $Y_2O_2^+$ are more complex than those of $Y_2O_3^+$ and $Y_3O_4^+$ which is consistent with multiple origins of $YO^+$ and $Y_2O_2^+$ (eqns. (5)–(8)).

*CAD of $Y_2O_3^+$*

The ion $Y_2O_3^+$ undergoes CAD quite readily to yield $YO^+$ and $Y_2O_2^+$ (Fig. 5). The intensity of the daughter ion $YO^+$ rises rapidly to 100% in the collision energy range 30–50 eV whereas $Y_2O_2^+$, the most favored product at low collision energy (up to 30 eV), posts a decreasing intensity with increasing collision energy. Both the intensities of $Y_2O_2^+$ and $Y_2O_3^+$ decrease with collision energy in a complex way with that of $Y_2O_3^+$ decreasing faster (Fig. 5). The ion $Y_2O_3^+$ therefore shows extreme vulnerability to CAD as:

$$Y_2O_3^+ \xrightarrow{-O} Y_2O_2^+ \qquad (9)$$

$$Y_2O_3^+ \xrightarrow{-YO_2} YO^+ \qquad (10)$$

Peaks due to $YO_2^+$ species were not observed. The monoxide $YO^+$ may also be obtained in secondary collisions involving $Y_2O_2^+$ (eqn. (11)):

$$Y_2O_2^+ \xrightarrow{-YO} YO^+ \qquad (11)$$

It is not possible to identify the most favorable reaction among (9)–(11) but (9) appears to have the least activation energy (Fig. 5). Plots of weighted intensities *versus* collision energy (not shown) show the intensity of $YO^+$ increasing curvilinearly with collision energy, which means $YO^+$ comes from several sources, in this case reactions (10) and (11). Most probably the primary CAD process (10) contributes more to the population of $YO^+$ than the secondary CAD process (11) since the intensity of $YO^+$ from parent ion $Y_2O_2^+$ (Fig. 6) exceeds that of the parent ion at much higher collision energies than found for $Y_2O_3^+$ (Fig. 5).

*CAD of $Y_2O_2^+$ and $YO^+$*

The ion $Y_2O_2^+$ has only one daughter ion $YO^+$ (eqn. (11)) the intensity of which increases almost linearly with collision energy (50–90 eV) (Fig. 6). By comparison $Y_2O_2^+$ is much more stable than the sesquioxide $Y_2O_3^+$ (Figs. 5 and 6). Using the slope of the linear plot of the intensity of $YO^+$ *versus* collision energy (Fig. 6) (1.5%/eV) as a guide to kinetic stability trends, the ion $Y_2O_2^+$ is as stable as the ion $Y_5O_7^+$ (slope of the $Y_3O_4^+$ (the major product) line is 2.5%/eV Fig. 2) although the appearance potentials of CAD products of $Y_5O_7^+$ are much higher (*vide infra*).

The ion $YO^+$ also has one daughter ion, $Y^+$, the intensity of which increases linearly with collision energy (50–110 eV) (Fig. 7) (slope 0.44%/eV) as expected for simple unimolecular collision activated dissociation. The CAD of $YO^+$ is slower at higher energies for reasons not clearly understood.

*CAD of Other Ions*

The intensity of $Y_4O_6^+$ was low and therefore only very prominent peaks rising well above the noise level were considered. The major CAD product of $Y_4O_6^+$ is $Y_3O_4^+$ with intensities at 100% throughout the entire collision energy range 30–110 eV.

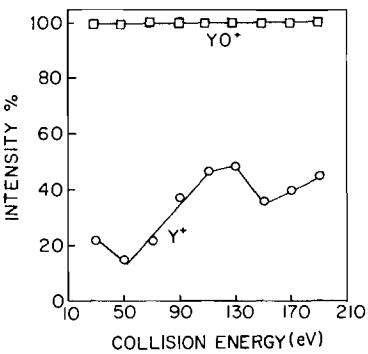


Fig. 7. Average CAD spectra of $YO^+$ intensities of daughter and parent ions *vs.* collision energy of $YO^+$.

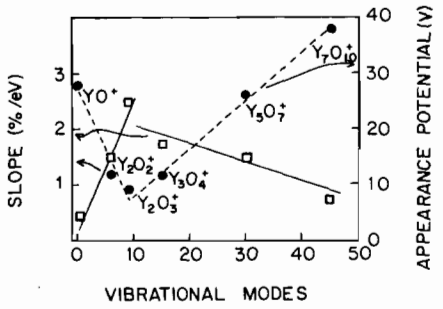


Fig. 8. Variations in appearance potentials (broken lines) of major CAD products of yttrium oxides and slopes of their linear intensity/collision energy plots (solid lines) with vibrational modes ($3n - 6$) of indicated parent ions.

The intensity of $Y_4O_6^+$ is varied as 40% (30 eV), 59% (50 eV), 51% (70 eV), 53% (90 eV) and 31% (110 eV). By comparison with $Y_3O_4^+$ and $Y_5O_7^+$, $Y_4O_6^+$ is very vulnerable to CAD just as the cation $Y_2O_3^+$ is; both $Y_4O_6^+$ and $Y_2O_3^+$ belong to the homologous series $Y_aO_{3a/2}^+$.

The major reaction is thus:

$$Y_4O_6^+ \xrightarrow{-YO_2} Y_3O_4^+ \qquad (12)$$

The intensity of $Y_6O_8^+$ was too low for systematic study but at 110 eV an intense peak due to $Y_5O_7^+$ was observed in the CAD spectrum. The major reaction is:

$$Y_6O_8^+ \xrightarrow{-YO} Y_5O_7^+ \qquad (13)$$

The peak due to $YO^+$ was not observed which means, that it cleaves off as a neutral species.

### *Appearance Potentials and Daughter Ion Intensity Dependence on Collision Energy*

The appearance potentials of the most prominent daughter ions produced in CAD processes in which at least one yttrium species separates from the parent ion are plotted against the number of vibrational modes given by $3n - 6$ ($n$ being the number of atoms in the ion) in Fig. 8. For this plot reaction (9) (*i.e.* the appearance potential of $Y_2O_2^+$ from $Y_2O_3^+$) was not considered, instead the appearance potential of $YO^+$ (eqns. (10) or (11)) was used. These appearance potentials were derived by extrapolation of the best linear relationships of the most prominent daughter ions to intensity zero % in Figs. 1–3, 5–7, and reading off the threshold collisional energies on the $x$-intercept.

The plot in Fig. 8 shows decreasing appearance potentials of $Y^+$ and $YO^+$ which are daughters of $YO^+$ and $Y_2O_2^+$ (eqn. (11)) and $Y_2O_3^+$ (eqn. (10)) respectively. Then the appearance potential of $YO^+$ from $Y_3O_4^+$ (eqn. (5)), $Y_3O_4^+$ from $Y_5O_7^+$ (eqn. (3)) and $Y_7O_{10}^+$ (eqn. (2)) take on an increasing trend. This is consistent with a decreasing Y–O bond order on going from $YO^+$ to $Y_2O_2^+$ and $Y_2O_3^+$. Beyond $Y_2O_3^+$ in which single Y–O bonds are probably the rule, internal energy generated on collision with argon is distributed among many vibrational modes. It therefore takes increasingly larger collision energies to accumulate enough internal energy in Y–O bonds to initiate CAD processes.

Once the threshold collision energies are exceeded, the variations in the intensities of the daughter ions with excess collision energy (slope of linear parts of intensity *versus* collision energy curves (Figs. 1–3, 5–7) are consistent with the above observation (Fig. 8). For each incremental unit of collision energy, CAD processes (excluding reaction (9)) become more favorable on going from $YO^+$ to $Y_2O_2^+$ and $Y_2O_3^+$, thereafter the larger oxide clusters become more resilient to collision and fewer collisions end up in CAD processes (Fig. 8).

However, this may as well reflect kinetic contributions which are not factored out in the data of Fig. 8.

## Discussion

The results presented above have shown conclusively that the ions of general formula $Y_aO_{(3a-1)/2}^+$ namely, $YO^+$, $Y_3O_4^+$, $Y_5O_7^+$ and $Y_7O_{10}^+$ which were prominent in the FAB mass spectra of yttrium compounds [1–3], are the most thermodynamically stable oxide clusters and the preferred CAD products for all ion clusters studied. The ion $Y_2O_2^+$ has considerable stability which is comparable to that of $Y_3O_4^+$ and $Y_5O_7^+$, but when it yields to CAD it gives $YO^+$, a member of the $Y_aO_{(3a-1)/2}^+$ homologous series as a major product. The ion $Y_6O_8^+$ which along with $Y_2O_2^+$ belongs to the series $Y_aO_{(3a-2)/2}^+$ yields $Y_5O_7^+$, also a member of the series $Y_aO_{(3a-1)/2}^+$. The behavior of $Y_2O_2^+$ and $Y_6O_8^+$ thus indicates that the thermodynamic stability order of the oxide clusters studied is $Y_aO_{(3a-1)/2}^+ > Y_aO_{(3a-2)/2}^+ > Y_aO_{3a/2}^+$. Although members of these three homologous series are derived by successive additions of $Y_2O_3$ to $YO^+$, $Y_2O_2^+$ and $Y_2O_3^+$ respectively, the operative CAD mechanisms reflect a decisive thermodynamic control so that formation of the most thermodynamically stable oxide is always preferred. Therefore $Y_aO_{(3a-1)/2}^+$ clusters eliminate, $Y_2O_3$, their building block, to yield lower members of the same homologous series, whereas $Y_aO_{3a/2}^+$ and $Y_aO_{(3a-2)/2}^+$ clusters eliminate $YO_2$ and $YO$ respectively to yield appropriate members of the $Y_aO_{(3a-1)/2}^+$ series. The lowest $Y_aO_{3a/2}^+$ member $Y_2O_3^+$ does have a lower activation energy CAD pathway (eqn. 9) in which an oxygen atom is eliminated to yield $Y_2O_2^+$ which is more stable.

The charge distribution among the CAD products is consistent with the Stevenson–Audier rule [8, 9], namely that a positive charge is retained by the species of lower ionization energy. Accordingly, the species $Y_aO_{(3a-1)/2}$ having one yttrium(II) retains the positive charge when $Y_aO_{3a/2}^+$ fragments eliminating neutral $YO_2$. Similarly when $Y_aO_{(3a-1)/2}^+$ fragments, the positive charge resides on a lower $Y_aO_{(3a-1)/2}$ member, rather than $Y_aO_{3a/2}$ (e.g. $Y_2O_3$ or $Y_4O_6$) which are lost as neutrals. For the members of $Y_aO_{(3a-2)/2}^+$ series which eliminate neutral YO species leaving a positive charge on a $Y_aO_{(3a-1)/2}$ species, it appears by this rule that YO (the lowest member of the later series) has a higher ionization energy.

The oxides $Y_aO_{3a/2}^+$ have an electron deficit whereas the oxides $Y_aO_{(3a-2)/2}^+$ have an electron surplus if trivalent yttrium is considered to be the most stable and therefore preferred valency of yttrium. Electron deficiency is thus associated with extreme oxide cluster instability, the fragmentation of which yields the oxide species of trivalent yttrium $Y_aO_{(3a-1)/2}^+$ which are most stable. Electron surplus is better tolerated, thus the oxides $Y_aO_{(3a-2)/2}^+$ have considerable stability but when they yield to CAD they eliminate a low valency oxide YO, to yield the stable oxide species of trivalent yttrium. Therefore non-trivalent yttrium centers in the oxides $Y_aO_{3a/2}^+$ and $Y_aO_{(3a-2)/2}^+$ are sources of instability. It will be interesting to see how the series $Ln_aO_a^+$ in which only one Ln is trivalent and the rest are divalent fits in this picture. It is now not clear whether $Y_2O_2^+$ has the behavior of $Y_aO_a^+$ or $Y_aO_{(3a-2)/2}^+$ species. To this extent, electronic properties appear to be playing a significant role in determining stability trends. The possible significance of Y–O bond order reflected in Fig. 8 indicates that covalency factors may be more important in the bonding and thermodynamic stability of gaseous yttrium oxide clusters than ionicity in Y–O bonds.

The preference for formation of $Y_3O_4^+$ shown by $Y_7O_{10}^+$ (eqn. (2)) and $Y_5O_7^+$ (eqn. (3)) by eliminating $Y_4O_6$ and $Y_2O_3$ respectively, suggests that $Y_3O_4^+$ is an important structural unit of the $Y_aO_{(3a-1)/2}^+$ oxide series. Since CAD processes of members of different homologous series lead to similar products, $Y_aO_{(3a-1)/2}^+$, rearrangements prior to CAD are expected to occur if structures of the oxide species vary fundamentally from one homologous series to another.

## Conclusions

Collision activated dissociation studies have established that oxide cluster ions of the type $Ln_aO_{(3a-1)/2}^+$, which are more prominent in the mass spectra of lanthanide compounds containing oxygen and CAD spectra of $Ln_aO_{(3a-1)/2}^+$, $Ln_aO_{3a/2}^+$ and $Ln_aO_{(3a-2)/2}^+$ oxo clusters, are the most thermodynamically stable. These studies also suggest that electronic effects have the largest influence on the stability of oxo cluster ions, the presence of Ln(II) or Ln(IV), Ln ≠ Eu, Sm, Yb, Ce, Tb, being detrimental to the stability of the oxide cluster species. The behaviors of samarium, europium and ytterbium which have readily accessible divalent states or cerium, praseodymium and terbium which have readily accessible tetravalent states are not inferable from the above studies. Separate studies are in progress for these elements.

## Acknowledgements

We thank the U.S. Government for an extended Fulbright Scholarship to I. A. Kahwa, and the University of Dar es Salaam, Tanzania for extending his study leave. The Finnigan Mat TSQ70 was purchased with support from NIH grant #SSS-1(E)1S10RR-02803-01.

## References

1 I. A. Kahwa, J. Selbin, T. C.-Y. Hsieh and R. A. Laine, *Inorg. Chim. Acta*, in press, and refs. therein.
2 I. A. Kahwa, J. Selbin, T. C.-Y. Hsieh and R. A. Laine, *Inorg. Chim. Acta, 118*, 179 (1986).
3 I. A. Kahwa, *Ph.D. Dissertation*, Louisiana State University, Baton Rouge, La., U.S.A., 1986.
4 R. J. Doyle, Jr., *Anal. Chem., 59*, 537 (1987).
5 R. J. Doyle, Jr., *35th ASMS Ann. Conf. Mass Spectrom. Allied Top.*, Denver, Colorado, May, 1987, paper No. RPA31.
6 I. A. Kahwa, F. R. Fronczek and J. Selbin, *Inorg. Chim. Acta, 82*, 167 (1984).
7 S. P. Sinha, *Struct. Bonding (Berlin), 25*, 70 (1976).
8 H. A. Audier, *Org. Mass Spectrom., 2*, 283 (1969).
9 D. P. Stevenson, *Disc. Faraday Soc., 10*, 35 (1951).